

From Turbulence to Landscapes: Universality of Logarithmic Mean Profiles in Bounded Complex Systems

Milad Hooshyar

Princeton Environmental Institute and Princeton Institute for International and Regional Studies, Princeton University, USA

Sara Bonetti

Department of Environmental Systems Science, ETH Zurich, Switzerland

Arvind Singh

Department of Civil, Environmental, and Construction Engineering, University of Central Florida, USA

Efi Foufoula-Georgiou

Department of Civil and Environmental Engineering and Department of Earth System Science, University of California, Irvine, USA

Amilcare Porporato*

Princeton Environmental Institute and Department of Civil and Environmental Engineering, Princeton University, USA

(Dated: January 4, 2022)

The logarithmic mean-velocity profile is a key experimental and theoretical result in wall-bounded turbulence. Similarly, here we show that the topographic surface emerging between parallel zero-elevation boundaries presents an intermediate region with a logarithmic mean-elevation profile. We use model simulations, which account for growth, erosion, and smoothing processes and give rise to complex topography with channel branching and fractal river networks, as well as data from a physical landscape-evolution experiment. Dimensional and self-similarity arguments are used to corroborate this finding. Our results suggest a universality of the logarithmic scaling in bounded complex systems out of equilibrium, of which landscape topography and turbulence are quintessential examples.

The striking channel and ridge patterns in the land surface emerge from a competition between growth and erosion, driven by external climatic and tectonic forcings, resulting in surfaces that exhibit several well-known scaling laws [1]. The complex networks of channels and their self-similar statistical properties have common features with other branch-forming systems [2, 3] and have become a key example of out-of-equilibrium systems in statistical physics [4–7]. The resemblance between the landscape self-similarity and the scale invariance observed in turbulence has been exploited to analyze landscape morphology [8, 9]. In particular, Bonetti *et al.* [10] emphasized the parallels between the channelization cascade and the hierarchical pattern formation toward finer scales observed in the non-equilibrium systems such as hydrodynamic turbulence [11–13].

Here this analogy between turbulence and landscape evolution is strengthened by the discovery of a logarithmic region in the mean-elevation profiles, which resembles the logarithmic scaling of the mean stream-wise velocity in the intermediate region of wall bounded turbulent flows [11, 14–16]. As well known, in wall-bounded turbulence the mixing-length argument by Prandtl [17] first justified a logarithmic velocity profile which was then generalized by means of dimensional analysis and similarity considerations [16, 18, 19]. The constancy of the

slope of the logarithmic profile, commonly denoted by $1/\kappa$, where κ is the von Karman’s constant, has been verified in numerous experimental and numerical studies [16, 20–22].

We establish the existence of a logarithmic region in mean-elevation profiles using a combination of numerical simulations, laboratory experiments, and dimensional considerations. For high erosion rates, we obtain mean-elevation profiles consisting of a linear part close to the fixed-elevation boundary, similar to the viscous sub-layer in turbulence [23], followed by a logarithmic profile in the intermediate distant from both the boundary and the central part of the domain, similar to the inertial sub-layer in turbulence [11, 24].

Governing equations. – The evolution of the land surface elevation in detachment-limited condition [25–27] results from a balance between diffusive soil creep, fluvial erosion, and uplift,

$$\frac{\partial z}{\partial t} = D\Delta z - Ka^m|\nabla z|^n + U, \quad (1)$$

where $z(x, y, t)$ is the surface elevation at time t and location (x, y) , D is soil diffusivity, and U is the tectonic uplift rate. The term $Ka^m|\nabla z|^n$ is a sink term, which quantifies fluvial erosion with parameters K , m , and n . The variable $a(x, y, t)$ is defined as the contributing area per unit contour-line length. The presence of a in Eq. (1) follows from a condition of steady-state water depth

* Corresponding author, aporpora@princeton.edu

generated by a unit rainfall rate under the assumption that water moves in the direction of the local slope with a constant velocity. As a result [10, 28], a is given by the equation

$$\nabla \cdot \left(a \frac{\nabla z}{|\nabla z|} \right) = -1. \quad (2)$$

By non-dimensionalizing the system of equations (1) and (2), [10] derived the dimensionless number χ which quantifies the relative impact of fluvial erosion to diffusive transport and uplift,

$$\chi = \frac{K l^{m+n}}{D^n U^{1-n}}, \quad (3)$$

where l is a typical length scale of the domain. In this study we focus on the case $n = 1$; different values of n do not qualitatively change our results, as discussed in the Supplemental Material.

In analogy with a channel flow between parallel plates, we numerically solved the system of equations (1) and (2) in a strip of land, unbounded in the x direction and with constant elevation at two sides, $z(x, 0) = z(x, l_y) = 0$ m, where l_y is the width in the direction y (see Fig. 1a and the Supplemental Material for more details on numerical simulations). After reaching steady state, the mean-elevation profile $\bar{z}(y)$ was obtained by averaging the z field along the x -axis for $100 \text{ m} \leq x \leq 600 \text{ m}$ (Fig. 1) to minimize the effect of l_x on the mean behavior of the surface. An example of mean-elevation profile (solid black line) and the ensemble of profiles (red lines) are shown in $y - z$ plane of Fig. 1.

Increasing χ (i.e., increasing relative magnitude of fluvial erosion) results in a more dissected surface with branching channels (see Bonetti *et al.* [10]). As shown in Fig. 2, for $\chi = 10$, the emerged surface is smooth with no channels as the diffusive transport is dominant and prevents the growth of instability and channel formation. In these conditions, the mean elevation profile can be obtained analytically for $m = n = 1$ in terms of a hypergeometric function [10]. As χ exceeds a critical value (≈ 37 from linear stability analysis for $m = n = 1$), parallel channels emerge and, with higher χ , the surface becomes further dissected with the development of secondary branches [10]. The formation of branching channels impacts the mean-elevation profile as shown in Fig. 2e – g. It is evident that as χ increases the profiles become more uniform, similar to the flattening of the mean-velocity profile with increasing Reynolds number in turbulence [29].

Dimensional Analysis and Self-Similarity. – When averaged along the x direction, the surface properties (e.g., elevation and slope) only depend on y . Therefore, the elevation field $z(x, y)$ can be decomposed into the sum of the mean elevation \bar{z} and fluctuations z' around the

mean, similarly to the Reynolds decomposition [8, 30],

$$z(x, y) = \bar{z}(y) + z', \quad (4)$$

where $\bar{z}(y) = \lim_{l_x \rightarrow \infty} \frac{1}{l_x} \int_0^{l_x} z(x, y) dx$. The mean slope of steady-state surface is controlled by the parameters which describe the diffusive transport, fluvial erosion, and tectonic activity (D , K , U , and m in Eq. (1) with $n = 1$), the distance y from the boundary, and two length scales in the y and z directions (l_y and z_*) [19],

$$\frac{d\bar{z}}{dy} = f_1(y, l_y, z_*, D, K, U, m). \quad (5)$$

Choosing y , D , and z_* as fundamental, dimensionally independent variables, the Pi-theorem yields

$$\frac{y}{z_*} \frac{d\bar{z}}{dy} = f_2\left(\frac{y}{l_y}, \frac{K y^{m+1}}{D}, \frac{U y^2}{D z_*}, m\right), \quad (6)$$

from which simple manipulation of the variables leads to

$$(m+1) \eta \frac{d\phi}{d\eta} = f_3(\eta, \chi, \zeta, m), \quad (7)$$

where χ is given in Eq. (3) with $n = 1$ and $l = l_y$ and $\phi = \frac{\bar{z}}{z_*}$ is the normalized mean elevation \bar{z} by a factor z_* which describes the overall elevation of the profile. Here, we used $z_* = \bar{z}_{max}$, where \bar{z}_{max} is the average elevation at the divide ($y = l_y/2$). The dimensionless value χ is a global quantity (independent of y) reflecting the relative impact of fluvial erosion to diffusive transport [10]. The quantity $\eta = \frac{K y^{m+1}}{D}$ is a local variable with a similar form as χ but capturing the local relative contribution of those two processes, while $\zeta = \frac{U l_y^2}{D z_*}$ describes the relative impact of tectonic uplift to diffusive transport.

In a system with relatively small diffusive transport and dominated by fluvial erosion and uplift, χ and ζ take high values. The same argument also applies to η except for locations close to the boundary. Thus, when the variables η , χ , and ζ reach such an asymptotic condition one may assume complete self-similarity [19] according to which the function f_3 is independent of these quantities

$$\eta \frac{d\phi}{d\eta} = \kappa(m), \quad (8)$$

where κ is only a function of m . Integrating Eq. (8) yields

$$\phi = \kappa(m) \ln \eta + C, \quad (9)$$

where C is independent of η but may still depend on m , χ , and ζ . Eq. (9) describes the logarithmic scaling of the mean-elevation profile with respect to η . The emergence

of such a logarithmic profile is expected in systems dominated by fluvial erosion and away enough from both the boundary and the center of symmetry (high χ , ζ , and η).

Logarithmic profile from simulations. – Fig. 3a-c shows the mean-elevation profile for a range of χ using dimensionless variables ϕ and η with $z_* = z_{max}$ in a semi-log space for $m = 0.5, 0.7$, and 0.9 . Given the symmetric simulation domain, here we show half of the profile corresponding to $0 \leq y \leq \frac{l_y}{2}$, i.e. from boundary to the main drainage divide. The tendency of the mean-elevation profile toward a flatter shape and the logarithmic scaling (linear segment in the semi-log space of Fig. 3a-c) clearly appear beyond a certain χ . The logarithmic fits to the intermediate segments of the profiles for $\chi = 2 \times 10^5$ are shown in Fig. 3a-c (refer to the Supplemental Material for details). For a given m and as χ increases, the logarithmic segments expand and their slope decreases with an asymptotic behavior in which κ approaches to a slope independent of χ for relatively high χ (see Fig. 3d).

Laboratory Experiments. – We also analyzed the data from a landscape evolution experiment performed using the eXperimental Landscape Evolution (XLE) facility in the St. Anthony Falls Laboratory at the University of Minnesota, described in details in the Supplemental Material [31, 32]. The parameters modulating fluvial erosion and diffusion needed to analyze the logarithmic scaling were estimated assuming a steady state governed by equations (1) and (2) with $n = 1$ as explained in the Supplemental Material. Having D , K , and m from the experimental surfaces, we computed the slope of the logarithmic profile κ for the 16 surfaces with the same optimization algorithm used to analyze the surfaces from numerical simulation. The surfaces from the physical experiment also contain the logarithmic scaling (see Fig. S1d and e) with slopes κ that lay close to the results from the numerical simulation (Fig. 3d).

Conclusions. – Inspired by the resemblance between the progressive surface dissection and flattening of mean-elevation profile with the turbulence cascade and the turbulence velocity profile [29, 30], we explored the existence of a logarithmic region in mean-elevation profile similar to the logarithmic scaling of stream-wise velocity in wall bounded turbulent flows [11, 16, 24, 33].

In turbulence, the logarithmic scaling in the inertial sub-layer is a fundamental result [14] associated to several other generic properties such as the nearly constant normalized Reynolds shear stresses [34], the balance of the production and dissipation of turbulent kinetic energy [33, 34], and a characteristic behavior in terms of turbulence energy cascade within the inertial sub-range [11]. Such a logarithmic scaling has also been reproduced under statistical stability through maximizing viscous dissipation [35, 36].

In landscape evolution, the existence of similar logarithmic scaling may also be justified by invoking a competition between surface forming mechanisms and the tendency toward an optimal state [1, 4, 5, 37]. The fact

that we found a logarithmic region in both a minimalist model of landscape evolution and in laboratory experiments hints at the generality of such a scaling. A similar robustness to both boundary conditions and physical processes is present in turbulent velocity profiles, where a logarithmic region appears in both smooth and rough walls, as well as within different levels of approximation (e.g., direct numerical simulations and large-eddy simulation) [15, 38, 39]. Finally, our results from numerical simulations show that the logarithmic scaling persists for a wide range of model parameters, in agreement with the existence of the logarithmic scaling in turbulent flow for different types of fluids (e.g., Newtonian and non-Newtonian) [40, 41]. In both turbulence and landscapes the logarithmic scaling emerges at an intermediate distance, when transitioning from an outer region toward the boundary. Landscapes and turbulence are quintessential examples of complex systems out-of-equilibrium, both exhibiting a cascade of patterns toward finer scales [10, 30]. Our results suggest a universality of the logarithmic scaling in such type of systems, where the progression of complexities (patterns) is prevented by the system boundary.

Acknowledgements. – A.P. acknowledges support from the US National Science Foundation (NSF) grants EAR-1331846 and EAR-1338694, and BP through the Carbon Mitigation Initiative (CMI) at Princeton University. M.H acknowledges support from the Princeton Institute for International and Regional Studies (PIIRS) and the Princeton Environmental Institute (PEI). E.F. acknowledges support from the US National Science Foundation (NSF) grants DMS-1839336, EAR-1242458, and EAR-1811909.

I. SUPPLEMENTAL MATERIAL

Here, we provide more details on the numerical and laboratory experiments used to establish the existence of the logarithmic scaling in mean-elevation profile. We also show the robustness of such scaling with respect to the parameter n (the exponent of slope in the governing equation).

A. Numerical Simulation

We solved numerically the equations (1) and (2) to examine the mean-elevation profile under different conditions of diffusive transport and fluvial erosion. The simulation domain was a 700 m by 100 m rectangular grid with constant elevation $z = 0$ m at the boundary, as shown in Fig. 1. This choice allowed us to neglect the effect of the domain dimension along the x axis, mimicking the case of an infinite strip.

We used the D_∞ flow-direction algorithm to efficiently calculate the contributing area at each pixel in the discretized domain and then divided it by grid size to com-

pute the specific catchment area a [10, 28, 42]. The spatial grid spacing was 1 m and the timestep of discretization Δt was selected small enough to avoid numerical instabilities. As initial condition, we used a tent-shaped surface plus random noise in which the local minima were filled. The steady-state condition was assumed to be reached when the average elevation change was less than 0.0001 of the change due to the uplift ($U\Delta t$). For the diffusion term we used an explicit central finite difference approximation in space and a forward approximation in time. We used a semi-implicit scheme for time integration of the sink term by iteratively processing computational nodes starting from the nodes at the boundary, with $z = 0$ m and no other node receiving their flow, and moving up toward the source nodes [43]. We performed simulations with $1 \leq \chi \leq 2 \times 10^5$, $0.1 \leq m \leq 1$, and $0.8 \leq n \leq 1.2$ to cover the range of parameters reported in the literature [27, 44]. For simplicity, we used $D = 0.005$ m²/yr and changed K to achieve desired χ for a given m value according to Eq. (3).

After reaching steady-state, we computed the characteristics of the logarithmic segment of the non-dimensional mean-elevation profile by fitting a function to the profile within $0 \leq y \leq l_y/2$. This includes a linear part for the segment close to the boundary and a logarithmic function for the intermediate segment. We also considered an additional power function for the segment close to the divide to cover the whole profile and close the fitting problem. We found the best fits by maximizing the summation of R^2 values of the fit to each segment. The variables for optimization are two thresholds on η which correspond to transition from the linear segment close to the boundary to the intermediate logarithmic segment, and the transition from logarithmic segment to the section close to the divide. Using such thresholds, simple linear regression gives the slope of the logarithmic profile denoted by κ (see Eq. (9)).

B. Laboratory Experiments

We also analyzed the data from a landscape evolution experiment performed using the eXperimental Landscape Evolution (XLE) facility in the St. Anthony Falls Laboratory at the University of Minnesota [31, 32]. The experiment consists of a 500 mm long, 500 mm wide, and 300 mm deep erosion box filled with a homogeneous mixture of fine silica and a surmounted rainfall simulator. The domain was subject to constant uplift rate ($U = 20$ mm/hr) and initial constant rainfall rate of $P = 45$ mm/hr which was increased to $P = 225$ mm/hr (see Fig. 4a). We analyzed 16 surfaces (0.5 mm by 0.5 mm Digital Elevation Models) scanned at 5 min intervals spanning 75 min of the simulation. The first 10 surfaces correspond to $P = 45$ mm/hr and the last 6

to $P = 225$ mm/hr. Fig. 4 shows two examples of the experimental surface.

The parameters modulating fluvial erosion and diffusion needed to analyze the logarithmic scaling were estimated assuming a steady state governed by equations (1) and (2) with $n = 1$ [44]. The specific catchment area a was computed by dividing the total contributing area from D_∞ by the grid spacing of the scanned surfaces (0.5 mm) [42]. Following Perron *et al.* [45] and focusing on the regions with small fluvial erosion (hilltops with small a and $|\nabla z|$), from Eq. (1), D was approximated as

$$D = -\frac{U}{\Delta z_{a|\nabla z| \rightarrow 0}}. \quad (10)$$

Given D in Eq. (1) at steady state, K and m can be estimated by fitting a power function to $\frac{D\Delta z + U}{|\nabla z|}$ versus a relationship [32, 45]

$$\frac{D\Delta z + U}{|\nabla z|} = Ka^m. \quad (11)$$

Having D , K , and m from the experimental surfaces, we computed the slope of the logarithmic profile κ for the 16 surfaces with the same optimization algorithm used to analyze the surfaces from numerical simulation. Examples of the fitted logarithmic profiles are shown in Fig. 4d and e.

C. The effect of n on the logarithmic scaling

Here, we investigate the controls of the parameter n in Eq. (1) on the characteristics of the logarithmic scaling of mean-elevation profile. The self-similarity arguments presented in the paper for $n = 1$ can be readily generalized with respect to n by defining $\eta = \frac{Ky^{m+n}}{D^n U^{1-n}}$ and using χ from Eq. (3) with $l = l_y$. Following the same line of reasoning, one can find

$$\phi = \kappa(m, n) \ln \eta + C, \quad (12)$$

where κ is a function of both m and n . To reveal details on the functional dependence of κ on n , we run an additional 300 simulations with $\chi \geq 10^4$, $m = 0.5, 0.7$, and 0.9 , $n = 0.8, 0.9, 1, 1.1$, and 1.2 , and the same boundary and initial condition discussed earlier. Our result clearly shows that, the logarithmic scaling emerges for a range of parameter n (Figure 5b and c) and the slope κ increases with higher n values (Fig. 5a).

-
- [1] I. Rodríguez-Iturbe and A. Rinaldo, *Fractal river basins: chance and self-organization* (Cambridge University Press, 2001).
- [2] S. Kramer and M. Marder, Evolution of river networks, *Physical Review Letters* **68**, 205 (1992).
- [3] A. Arneodo, F. Argoul, E. Bacry, J. Muzy, and M. Tabard, Golden mean arithmetic in the fractal branching of diffusion-limited aggregates, *Physical review letters* **68**, 3456 (1992).
- [4] K. Sinclair and R. C. Ball, Mechanism for global optimization of river networks from local erosion rules, *Physical Review Letters* **76**, 3360 (1996).
- [5] A. Rinaldo, A. Maritan, F. Colaiori, A. Flammini, R. Rigon, I. Rodríguez-Iturbe, and J. R. Banavar, Thermodynamics of fractal networks, *Physical review letters* **76**, 3364 (1996).
- [6] J. R. Banavar, F. Colaiori, A. Flammini, A. Giacometti, A. Maritan, and A. Rinaldo, Sculpting of a fractal river basin, *Physical review letters* **78**, 4522 (1997).
- [7] J. R. Banavar, F. Colaiori, A. Flammini, A. Maritan, and A. Rinaldo, Scaling, optimality, and landscape evolution, *Journal of Statistical Physics* **104**, 1 (2001).
- [8] C. Paola, Incoherent structure: turbulence as a metaphor for stream braiding, Coherent flow structures in open channels **65**, 705 (1996).
- [9] P. Passalacqua, F. Porté-Agel, E. Foufoula-Georgiou, and C. Paola, Application of dynamic subgrid-scale concepts from large-eddy simulation to modeling landscape evolution, *Water Resources Research* **42** (2006).
- [10] S. Bonetti, M. Hooshyar, C. Camporeale, and A. Porporato, Channelization cascade, arXiv e-prints, arXiv:1812.03696 (2019), arXiv:1812.03696 [physics.geoph].
- [11] H. Tennekes, J. L. Lumley, J. Lumley, *et al.*, *A first course in turbulence* (MIT press, 1972).
- [12] G. R. Chavarria, C. Baudet, and S. Ciliberto, Hierarchy of the energy dissipation moments in fully developed turbulence, *Physical review letters* **74**, 1986 (1995).
- [13] A. Frishman and C. Herbert, Turbulence statistics in a two-dimensional vortex condensate, *Physical review letters* **120**, 204505 (2018).
- [14] P. Bradshaw and G. P. Huang, The law of the wall in turbulent flow, *Proceedings of the Royal Society of London. Series A: Mathematical and Physical Sciences* **451**, 165 (1995).
- [15] J. Jiménez, Cascades in wall-bounded turbulence, *Annual Review of Fluid Mechanics* **44**, 27 (2012).
- [16] P. Luchini, Universality of the turbulent velocity profile, *Physical review letters* **118**, 224501 (2017).
- [17] L. Prandtl, 7. bericht uber untersuchungen zur ausgebildeten turbulenz, *ZAMM-Journal of Applied Mathematics and Mechanics/Zeitschrift für Angewandte Mathematik und Mechanik* **5**, 136 (1925).
- [18] C. M. Millikan, A critical discussion of turbulent flows in channels and circular tubes, in *Proceedings of the 5th International Congress of Applied Mechanics*, Harvard University and MIT (Wiley Online Library, 1938).
- [19] G. I. Barenblatt, *Scaling, self-similarity, and intermediate asymptotics: dimensional analysis and intermediate asymptotics*, Vol. 14 (Cambridge University Press, 1996).
- [20] J. Nikuradse, Gesetzmäßigkeiten der turbulenten strömung in glatten rohren (nachtrag), *Forschung im Ingenieurwesen* **4** (1933).
- [21] J. G. M. Eggels, F. Unger, M. H. Weiss, J. Westerweel, R. J. Adrian, R. Friedrich, and F. T. M. Nieuwstadt, Fully developed turbulent pipe flow: a comparison between direct numerical simulation and experiment, *Journal of Fluid Mechanics* **268**, 175210 (1994).
- [22] S. C. C. Bailey, M. Vallikivi, M. Hultmark, and A. J. Smits, Estimating the value of von krmns constant in turbulent pipe flow, *Journal of Fluid Mechanics* **749**, 7998 (2014).
- [23] B. J. McKeon, J.-d. Li, W. Jiang, J. F. Morrison, and A. J. Smits, Further observations on the mean velocity distribution in fully developed pipe flow, *Journal of Fluid Mechanics* **501**, 135 (2004).
- [24] I. Marusic, J. P. Monty, M. Hultmark, and A. J. Smits, On the logarithmic region in wall turbulence, *Journal of Fluid Mechanics* **716** (2013).
- [25] A. D. Howard, A detachment-limited model of drainage basin evolution, *Water resources research* **30**, 2261 (1994).
- [26] N. Izumi and G. Parker, Inception of channelization and drainage basin formation: upstream-driven theory, *Journal of Fluid Mechanics* **283**, 341 (1995).
- [27] J. T. Perron, W. E. Dietrich, and J. W. Kirchner, Controls on the spacing of first-order valleys, *Journal of Geophysical Research: Earth Surface* **113** (2008).
- [28] S. Bonetti, A. Bragg, and A. Porporato, On the theory of drainage area for regular and non-regular points, *Proceedings of the Royal Society A: Mathematical, Physical and Engineering Sciences* **474**, 20170693 (2018).
- [29] P. K. Kundu, I. M. Cohen, and D. W. Dowling, *Fluid Mechanics 5th ed.* (Elsevier, 2011).
- [30] O. Reynolds, Iv. on the dynamical theory of incompressible viscous fluids and the determination of the criterion, *Philosophical transactions of the royal society of london.(a.)*, 123 (1895).
- [31] A. Singh, L. Reinhardt, and E. Foufoula-Georgiou, Landscape reorganization under changing climatic forcing: Results from an experimental landscape, *Water Resources Research* **51**, 4320 (2015).
- [32] M. Hooshyar, A. Singh, D. Wang, and E. Foufoula-Georgiou, Climatic controls on landscape dissection and network structure in the absence of vegetation, *Geophysical Research Letters* **46**, 3216 (2019).
- [33] T. Banerjee and G. Katul, Logarithmic scaling in the longitudinal velocity variance explained by a spectral budget, *Physics of Fluids* **25**, 125106 (2013).
- [34] S. B. Pope, *Turbulent flows* (2001).
- [35] W. Malkus and L. Smith, Upper bounds on functions of the dissipation rate in turbulent shear flow, *Journal of Fluid Mechanics* **208**, 479 (1989).
- [36] J. Bertram, Maximum kinetic energy dissipation and the stability of turbulent poiseuille flow, *Journal of Fluid Mechanics* **767**, 342 (2015).
- [37] R. Rigon, A. Rinaldo, I. Rodríguez-Iturbe, R. L. Bras, and E. Ijjasz-Vasquez, Optimal channel networks: a framework for the study of river basin morphology, *Water Resources Research* **29**, 1635 (1993).
- [38] J. Kim, P. Moin, and R. Moser, Turbulence statistics in fully developed channel flow at low reynolds number,

- Journal of fluid mechanics **177**, 133 (1987).
- [39] W. Cheng and R. Samtaney, Power-law versus log-law in wall-bounded turbulence: A large-eddy simulation perspective, *Physics of Fluids* **26**, 011703 (2014).
 - [40] K. C. Wilson and A. D. Thomas, A new analysis of the turbulent flow of non-newtonian fluids, *The Canadian Journal of Chemical Engineering* **63**, 539 (1985).
 - [41] M. Rudman and H. M. Blackburn, Direct numerical simulation of turbulent non-newtonian flow using a spectral element method, *Applied mathematical modelling* **30**, 1229 (2006).
 - [42] D. G. Tarboton, A new method for the determination of flow directions and upslope areas in grid digital elevation models, *Water resources research* **33**, 309 (1997).
 - [43] J. Braun and S. D. Willett, A very efficient $O(n)$, implicit and parallel method to solve the stream power equation governing fluvial incision and landscape evolution, *Geomorphology* **180**, 170 (2013).
 - [44] K. Sweeney, J. Roering, and C. Ellis, Experimental evidence for hillslope control of landscape scale, *Science* **349**, 51 (2015).
 - [45] J. T. Perron, J. W. Kirchner, and W. E. Dietrich, Formation of evenly spaced ridges and valleys, *Nature* **460**, 502 (2009).

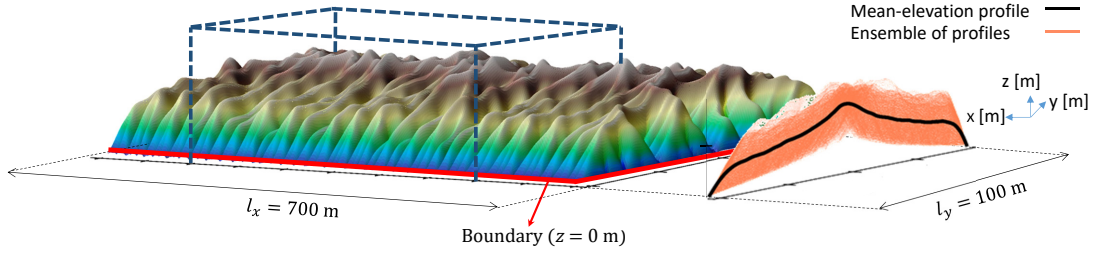


FIG. 1. An example of the steady-state surface from the numerical solution of equations (1) and (2). The simulation domain is $l_x = 700$ m by $l_y = 100$ m and has 1 m grid spacing. The boundary conditions at the edges are constant elevation $z = 0$ m. On the $y - z$ plane, the mean-elevation profile and the ensemble of profiles are shown. To minimize the effect of domain size along x-axis, for further analysis we used the surface within $100 \text{ m} \leq x \leq 600 \text{ m}$ as highlighted by the box.

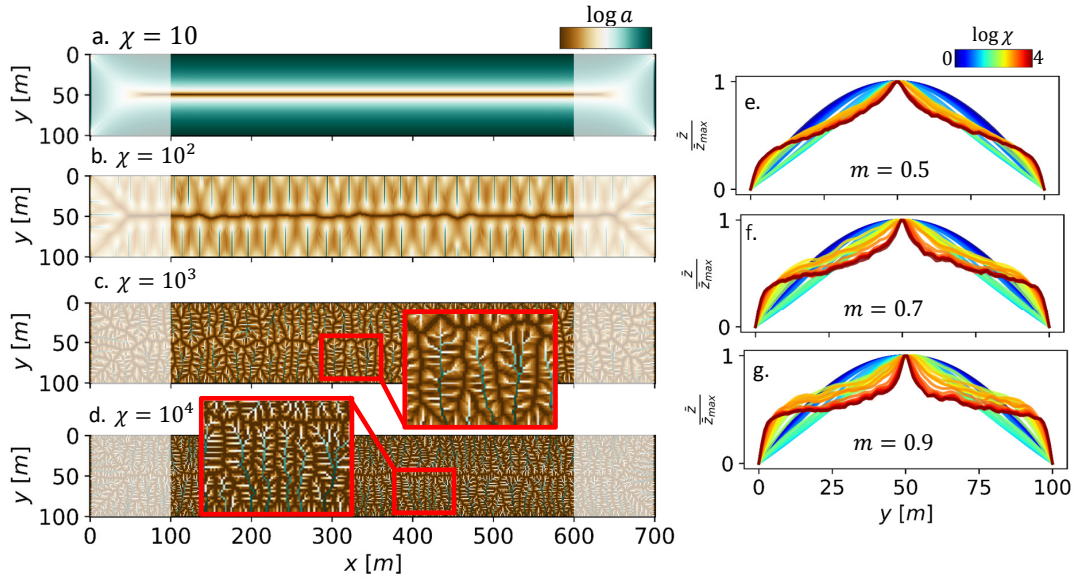


FIG. 2. The landscape surface and mean-elevation profile for different χ and m . (a-d) The specific catchment area a for $\chi = 10$, 10^2 , 10^3 , and 10^4 and $m = 0.5$. The shaded segments at the boundaries are discarded for further extraction of mean-elevation profiles. The red boxes in c and d show zoomed-in channel patterns in the marked portions of the domain. (e-g) The average profile for a wide range of χ and $m = 0.5$, $m = 0.7$, and $m = 0.9$. As χ increases (higher relative proportion of fluvial erosion to diffusive transport), the surface becomes more dissected with branching channels. This results in the evolution of the mean-elevation profile toward a flatter shape.

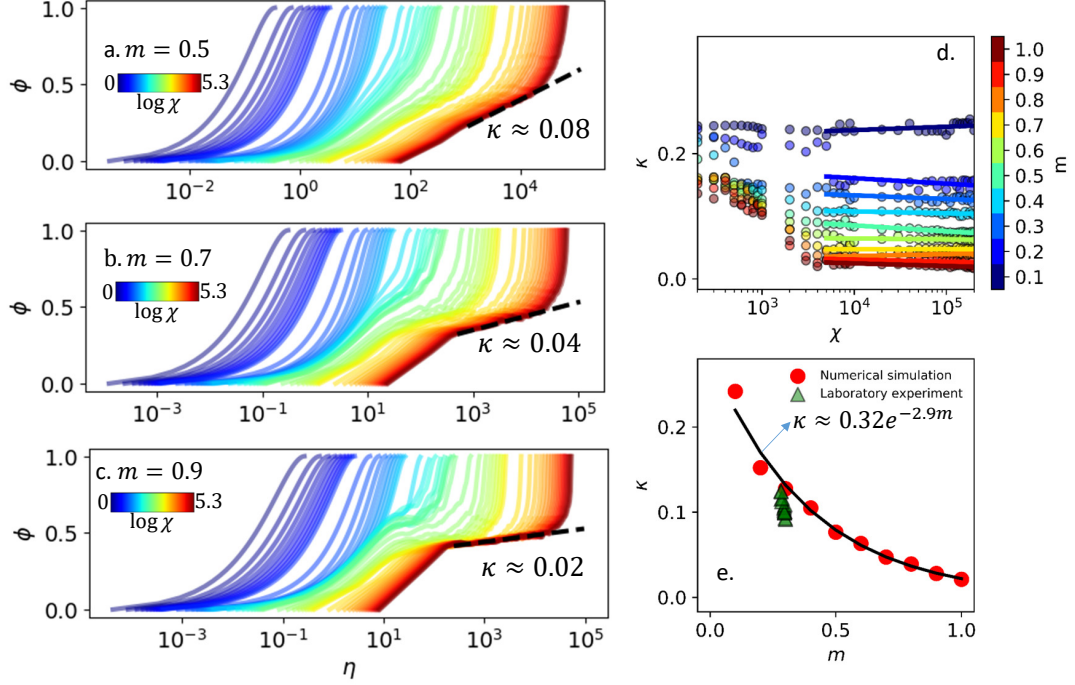


FIG. 3. The logarithmic profile in numerical simulations. (a-c) The dimensionless profiles corresponding to $0 \leq y \leq l_y/2$ in a semi-log space for $m = 0.5$, 0.7 , and $m = 0.9$. The dimensionless quantities are defined as $\eta = \frac{Ky^{m+1}}{D}$ and $\phi = \frac{z}{z_*}$ with $z_* = \bar{z}_{max}$. Increasing χ leads to the emergence and further expansion of the logarithmic segment in the profiles. The dashed lines are the fitted logarithmic lines to the profiles with $\chi = 2 \times 10^5$ and their slopes are reported as κ . (d) The slope κ of the logarithmic segment versus χ for different m . The slope κ shows an asymptotic behavior with respect to χ and is independent of χ for relatively high χ . The lines show the linear fits to the (χ, κ) data points for $\chi \geq 10^4$ at a given m and their negligible slope confirms that κ is independent of χ for relatively high χ . (e) The relationship between κ and m . The slope κ (average of simulations with $\chi \geq 10^4$) decreases monotonically with m meaning that higher values of m result in flatter logarithmic profile. The data points from a physical experiment (refer to the Supplemental Material for details) are also shown and lay close to the results from the numerical simulation.

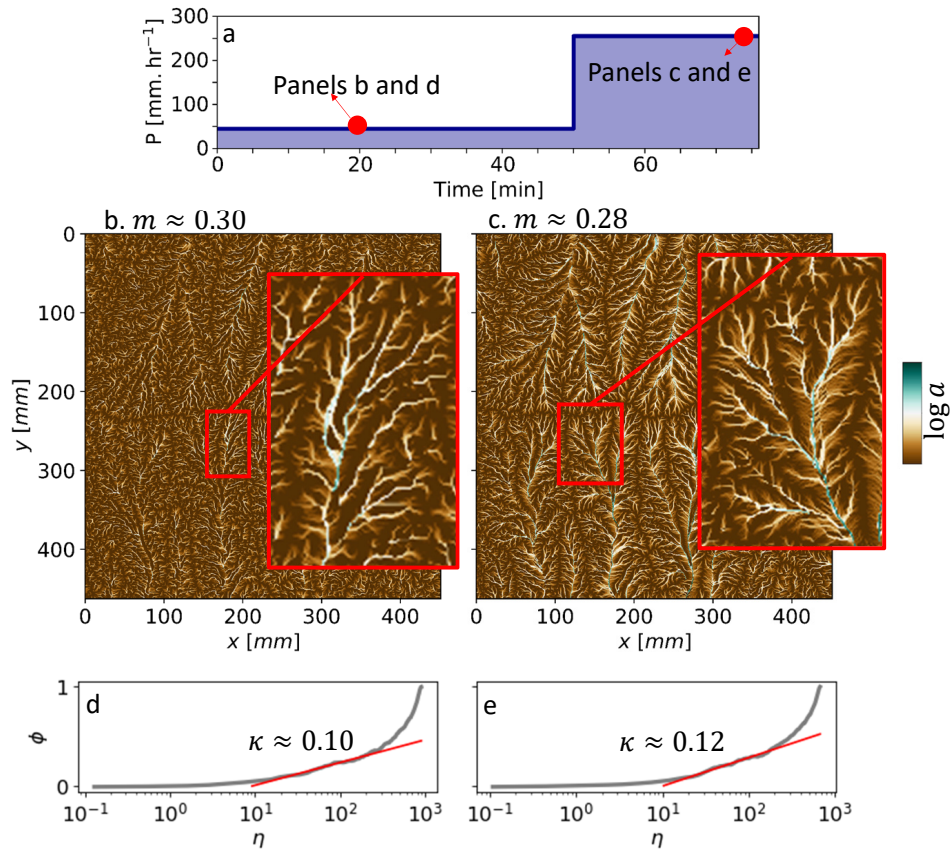


FIG. 4. The logarithmic profile from the experimental landscape. (a) The time variation of rainfall throughout the simulation. The experiment was started with $P = 45$ mm/hr which was increased to $P = 225$ mm/hr. (b and c) The specific catchment area a for two surfaces marked in (a). (d and e) The mean-elevation profile represented by the non-dimensional quantities η and ϕ . The fitted lines to the logarithmic segment of the profiles are shown by the red lines with the slope reported as κ .

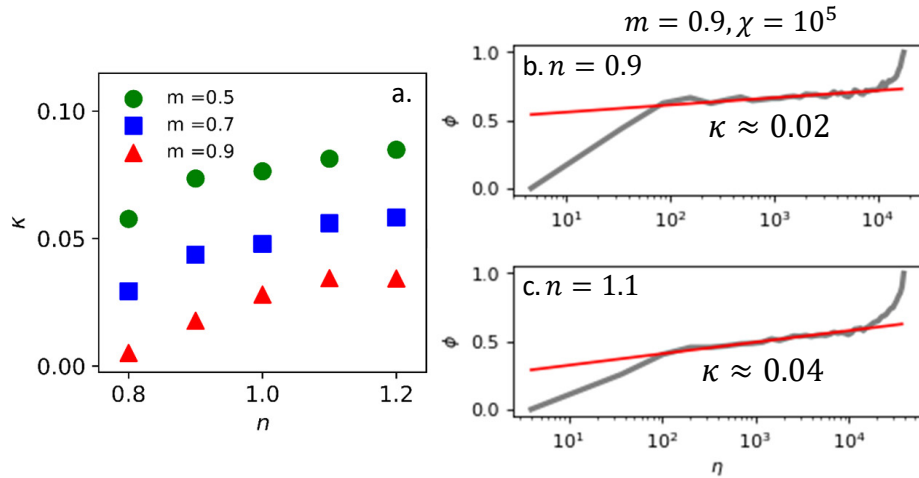


FIG. 5. The dependence of the slope of logarithmic scaling on the parameter n . (a) The logarithmic scaling persists for a range of n and the slope κ increases with higher n . (b and c) The non-dimensionalized mean-elevation profiles for two cases with the same $m = 0.9$ and $\chi = 10^5$, but different n . In both cases the logarithmic scaling is easily detectable.